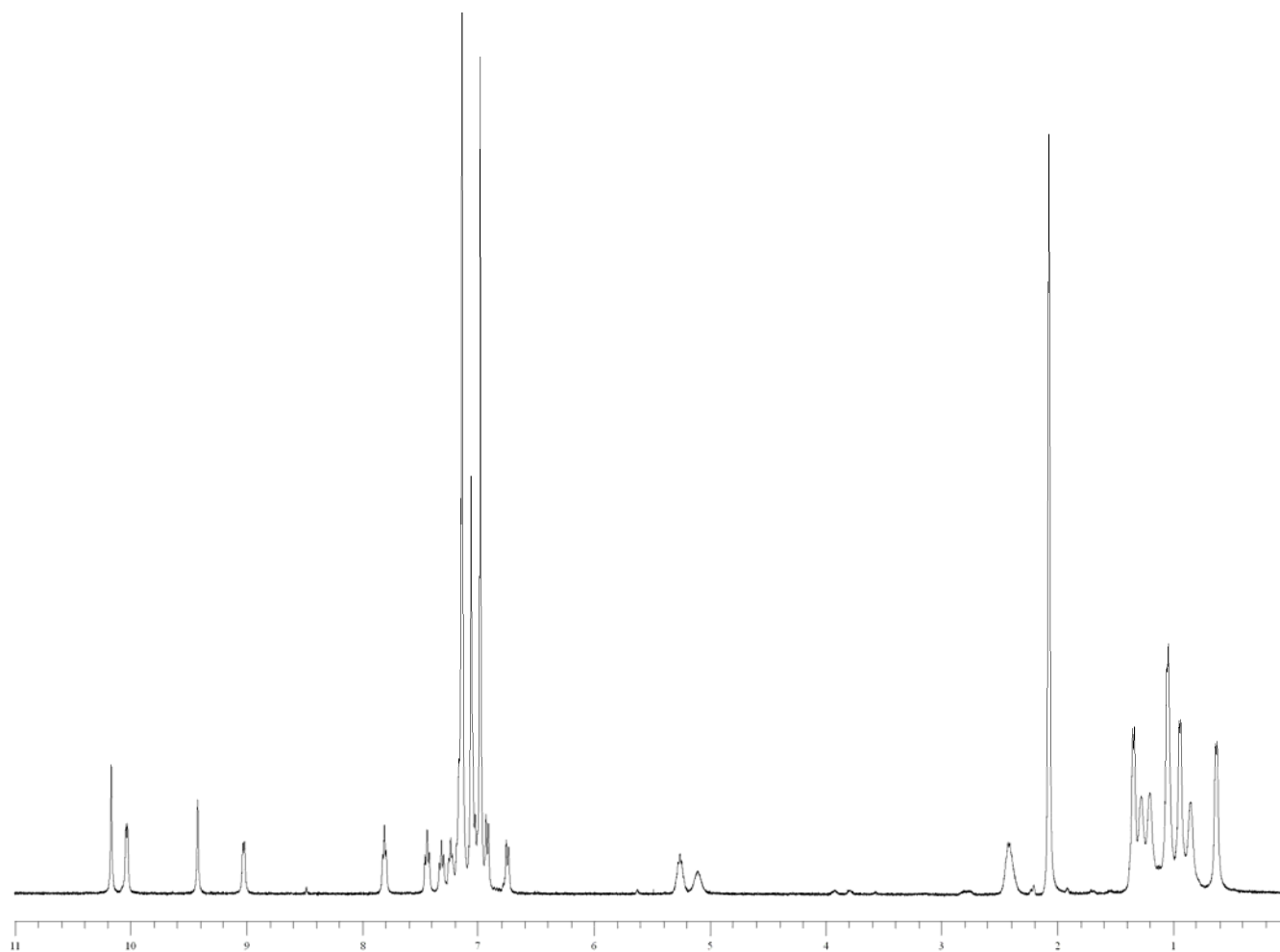


**Neutral Bis(α -iminopyridine)metal Complexes of the First-row Transition Ions
(Cr, Mn, Fe, Co, Ni, Zn) and Their Monocationic Analogues: Mixed Valency
Involving a Redox Non-innocent Ligand System**

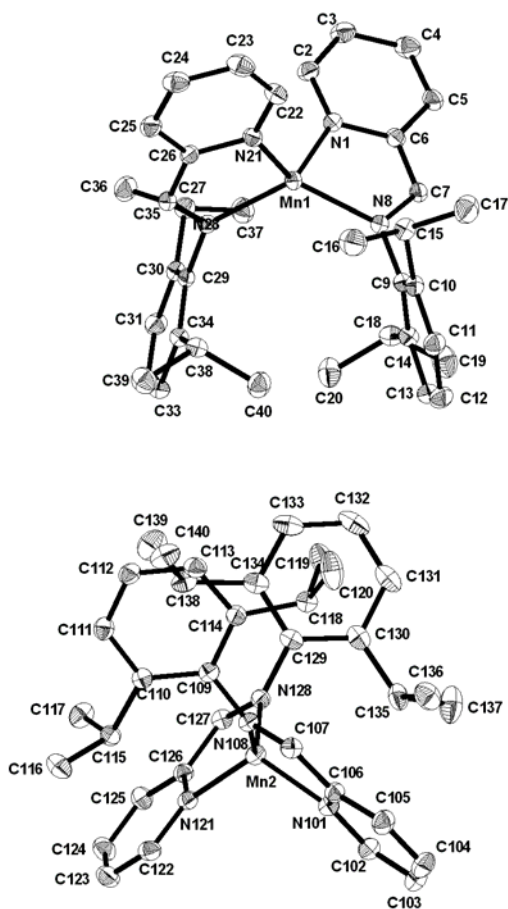
Supporting Information

Connie C. Lu; Eckhard Bill; Thomas Weyhermüller; Eberhard Bothe; Karl Wieghardt*

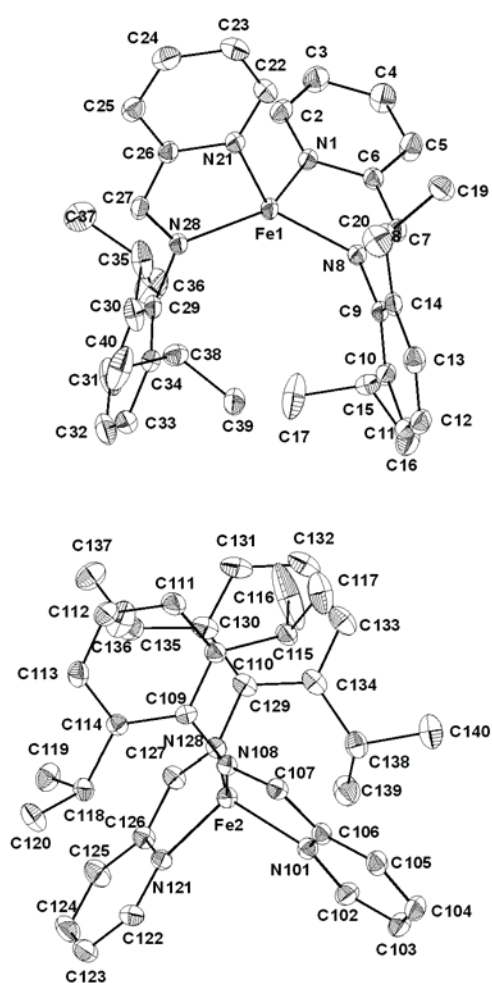


SI Figure 1. Proton NMR spectrum of $(L^*)_2Ni$ **5** in d_8 -toluene at -60 °C.

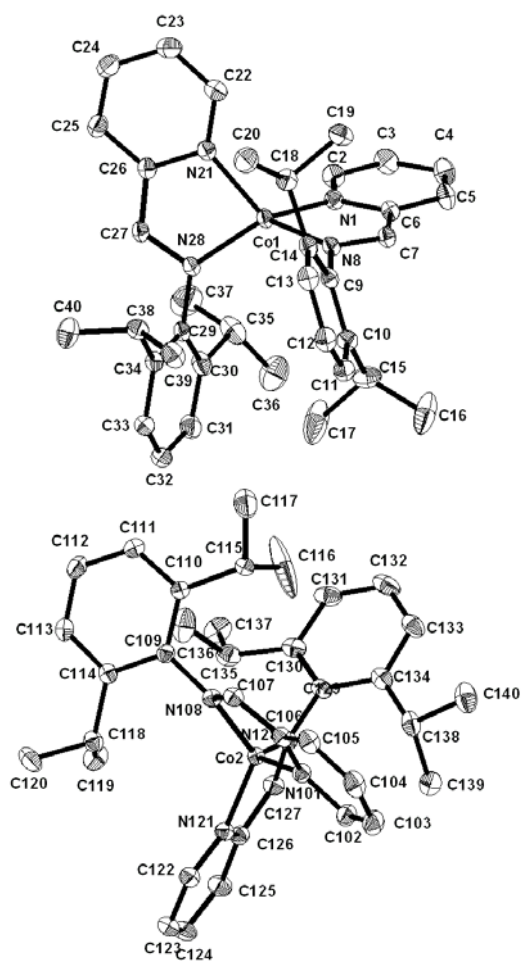
SI Figure 2. Thermal ellipsoid representation (50 %) of the neutral manganese complex **2** (two independent molecules). Hydrogen atoms have been omitted.



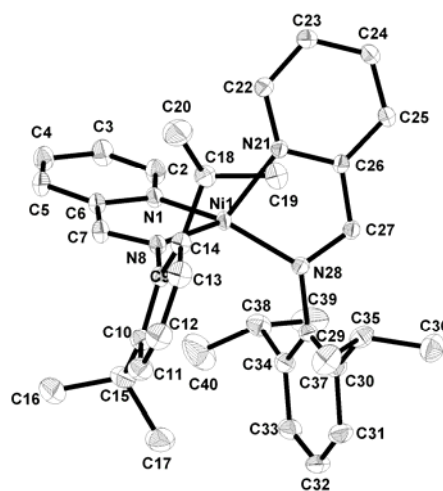
SI Figure 3. Thermal ellipsoid representation (50 %) of the neutral iron complex **3** (two independent molecules). Hydrogen atoms have been omitted.



SI Figure 4. Thermal ellipsoid representation (50 %) of the neutral cobalt complex **4** (two independent molecules). Hydrogen atoms have been omitted.



SI Figure 5. Thermal ellipsoid representation (50 %) of the neutral nickel complex **5**. Hydrogen atoms have been omitted.

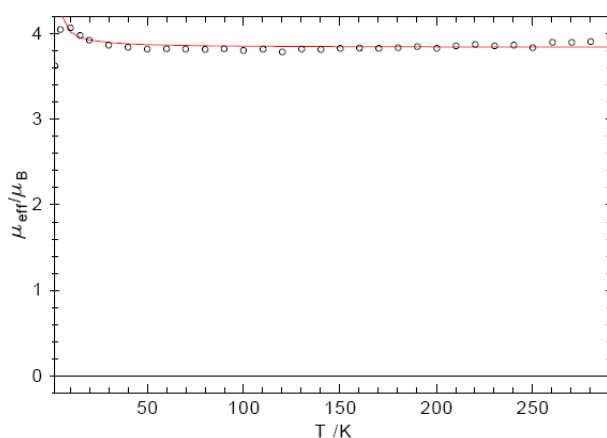


SI Figure 6. Estimation of Error in g Values Obtained from Modeling of Magnetic Data

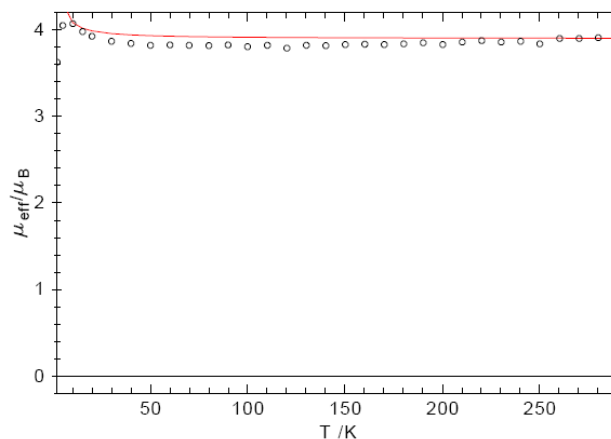
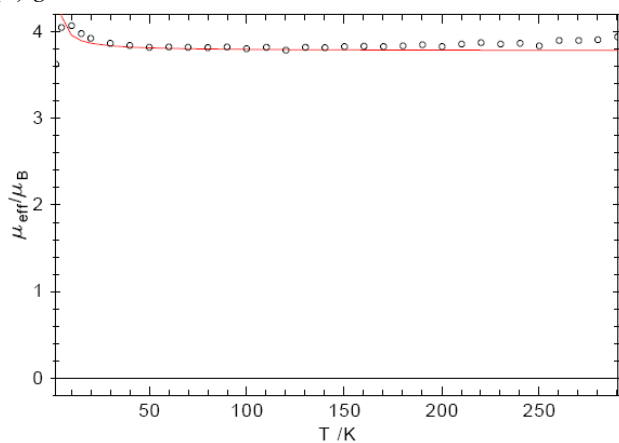
The modeling of the magnetic susceptibility data was performed using the program julX (Eckhard Bill, Max Planck Institute, Mülheim, Germany, December 2005). Parameters such as g values were optimized using a SIMPLEX procedure. The “error” in the g -value is not explicitly determined but can be estimated as ± 0.03 to ± 0.05 (depending on the quality of the data). *For example*, the magnetic data for the manganese complex **2** was well-fitted with $g = 1.98$ (a). Below are additional simulations wherein the g values are forcibly changed to (b) 1.95 and (c) 2.01. These latter simulations are worse fits in that fewer data points are touched by the fitted lines.

Another method to estimate the “error” in g values obtained from simulations of magnetic susceptibility data is to compare the g value obtained from EPR spectroscopy (when available, and independently simulated) due to the higher accuracy of the latter method. In this paper, we have done this comparison for (1) $(L^*)_2Co$ and (2) $[(L)_2Ni]^+ / [(L)_2Ni(THF)]^+$ (See SI Figures 7 and 13, respectively). For both of these complexes, the g values obtained from modeling of the magnetic measurements and EPR spectroscopy were within 0.05.

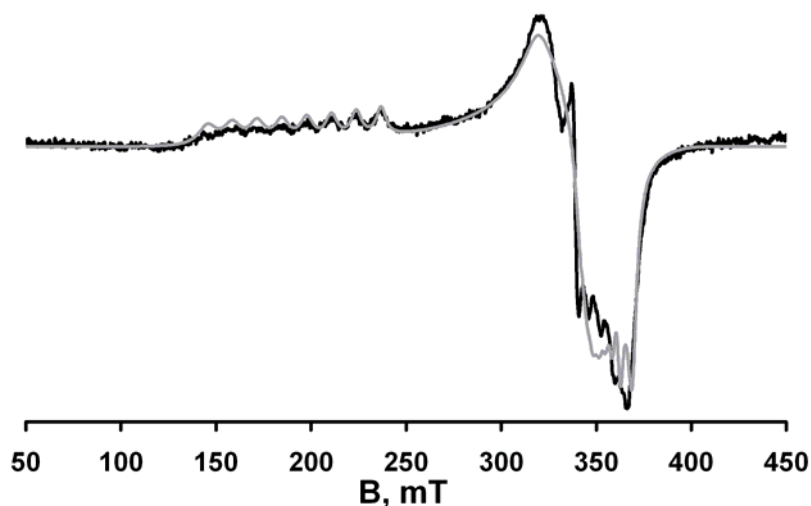
(a) $g = 1.98$ (reported value)



(b) $g = 1.95$

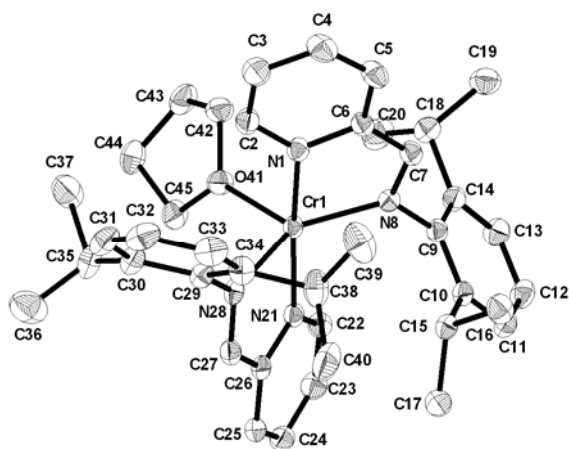


(c) $g = 2.01$

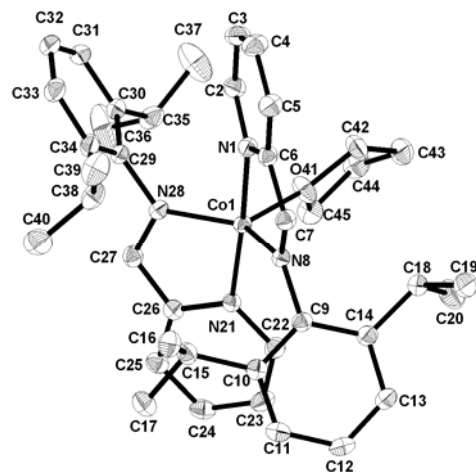


SI Figure 7. X-band EPR spectrum (dX''/dB) of Co **4** in toluene glass (1.0 mM, 11.0 K, frequency = 9.45 GHz, modulation = 16.0 G, power = 502 μ W). The spectrum was simulated by adopting the following values: $g = (2.05, 1.91, 3.53)$; line-widths, $\Gamma_{\text{freq}} = 100$ G, $\Gamma_{\text{field}} = (140, 37, 26)$ G, and line-width strain $c = (0, 0, 10)$ G; magnetic hyperfine coupling constants, $A(^{59}\text{Co}, I = 7/2) = (25, 30, 140) \times 10^4 \text{ cm}^{-1}$. Using the formula, $g_{\text{ave}} = \sqrt{\frac{(g_1^2 + g_2^2 + g_3^2)}{3}}$, g_{ave} is calculated to be 2.60. This is in good agreement with the g_{iso} value of 2.65 obtained from the magnetic susceptibility measurement of **4**. The features from 320 to 360 mT were ill-fitted due to “smearing” in the experimental data resulting from intermolecular interactions.

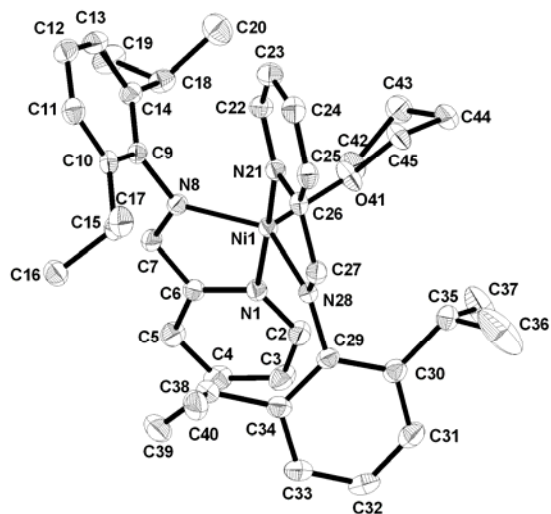
SI Figure 8. Thermal ellipsoid representation (50 %) of the cationic Cr complex $1^{ox} \cdot THF$. Hydrogen atoms and the $B(Ar_F)_4$ counteranion have been omitted.



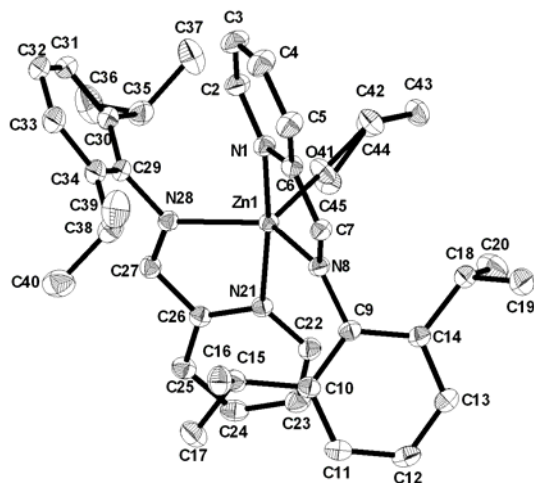
SI Figure 9. Thermal ellipsoid representation (50 %) of the cationic Co complex $4^{ox} \cdot THF$. Hydrogen atoms and the $B(Ar_F)_4$ counteranion have been omitted.



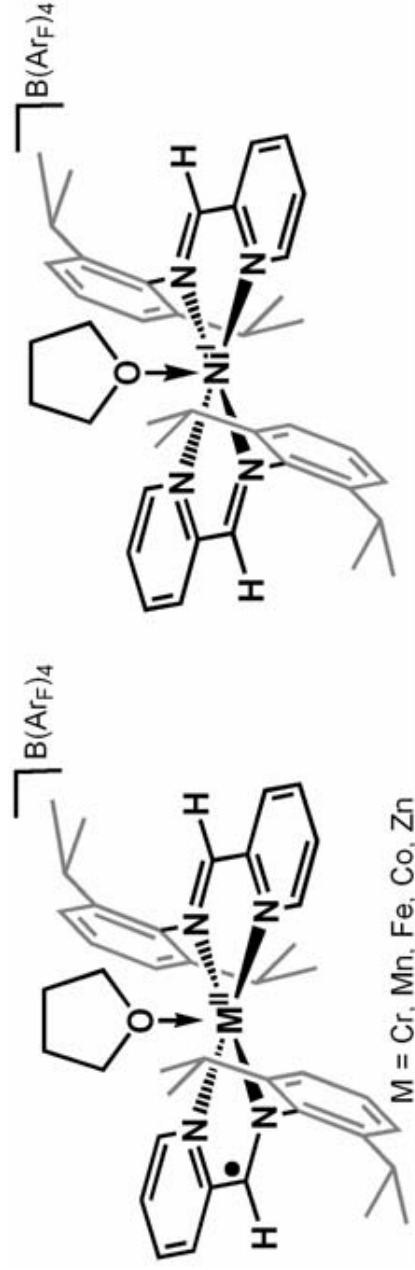
SI Figure 10. Thermal ellipsoid representation (50 %) of the cationic Ni complex **5^{ox}**•THF. Hydrogen atoms and the B(Ar_F)₄ counteranion have been omitted.



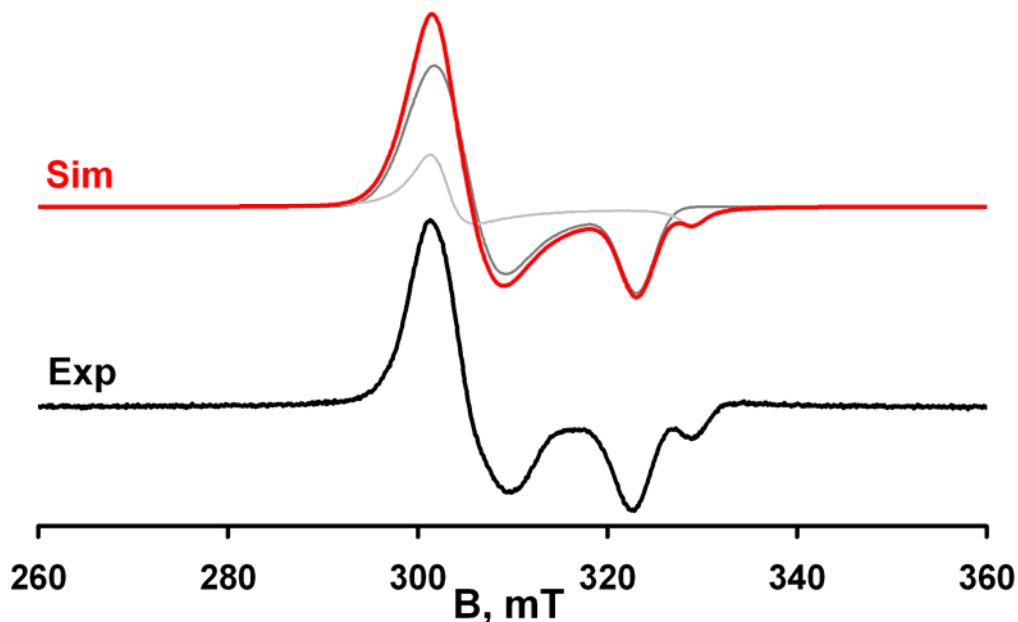
SI Figure 11. Thermal ellipsoid representation (50 %) of the cationic Zn complex **6^{ox}**•THF. Hydrogen atoms and the B(Ar_F)₄ counteranion have been omitted.



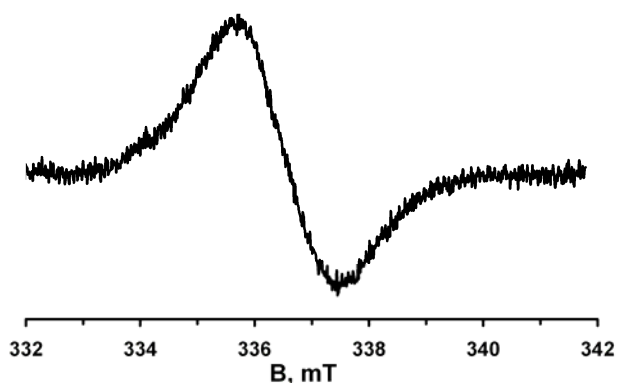
SI Figure 12. Bond Distances and Angles Around the Metal Center in $1^{ox} \cdot THF - 6^{ox} \cdot THF$



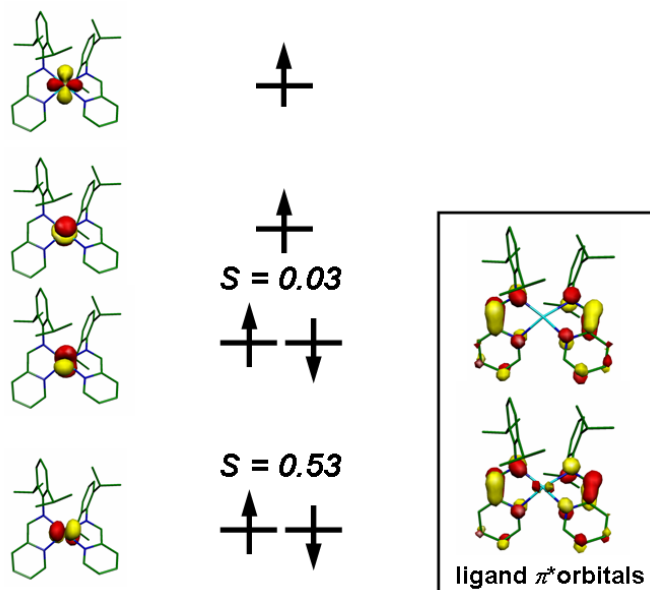
	Cr	Mn	Fe	Co	Ni	Zn
O-M-N_{py}	96.93(7) [°] 90.71(6) [°]	101.03(6) [°] 90.38(5) [°]	95.82(6) [°] 92.12(6) [°]	93.04(6) [°] 91.20(6) [°]	93.50(6) [°] 90.39(6) [°]	96.46(5) [°] 89.20(5) [°]
O-M-N_{im}	117.94(7) [°] 103.10(6) [°]	119.43(6) [°] 108.95(6) [°]	117.69(6) [°] 110.49(6) [°]	116.18(6) [°] 105.67(6) [°]	119.14(7) [°] 105.84(6) [°]	117.86(5) [°] 106.51(5) [°]
N_{im}-M-N_{im}	138.92(7) [°]	131.22(6) [°]	131.81(7) [°]	138.15(6) [°]	135.02(6) [°]	135.29(5) [°]
N_{py}-M-N_{py}	171.93(7) [°]	168.02(6) [°]	171.93(7) [°]	175.60(6) [°]	175.84(7) [°]	173.38(5) [°]
M-O	2.169(2) Å	2.126(1) Å	2.060(1) Å	2.115(1) Å	2.138(1) Å	2.076(1) Å



SI Figure 13. X-band EPR spectrum (dX''/dB) of $\text{Ni } 5^{\text{ox}}\cdot\text{THF}$ in frozen THF (1.0 mM, 10.0 K, frequency = 9.45 GHz, modulation = 10.0 G, power = 252 μW). The spectrum is a composite of two species. Based on the g values, these species are similar and are likely two geometric isomers (perhaps due to different orientations of the THF ring). The first species (shown in dark grey, 65%) was simulated by adopting the following values: $g = (2.23, 2.22, 2.09)$; line-widths, $\Gamma = (91, 83, 48)$ G. The second species (shown in light grey, 35%) was simulated with $g = (2.24, 2.23, 2.05)$; line-widths, $\Gamma = (62, 57, 42)$ G. The experimental g_{ave} based on EPR is 2.18, which is very close to the experimental g_{iso} value of 2.23 from the simulations of the magnetic susceptibility data (See Results and Discussion, Section 2.6).

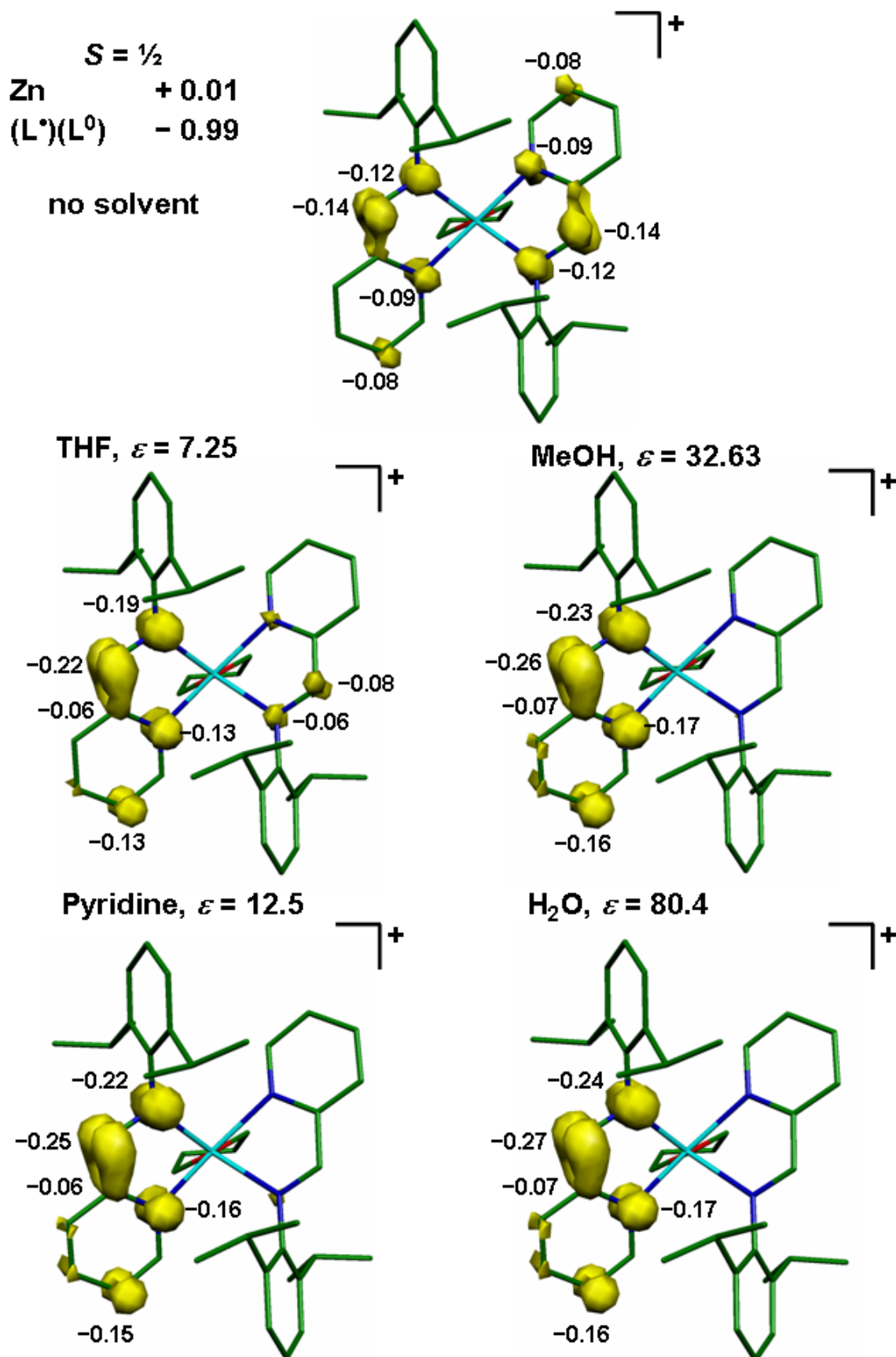


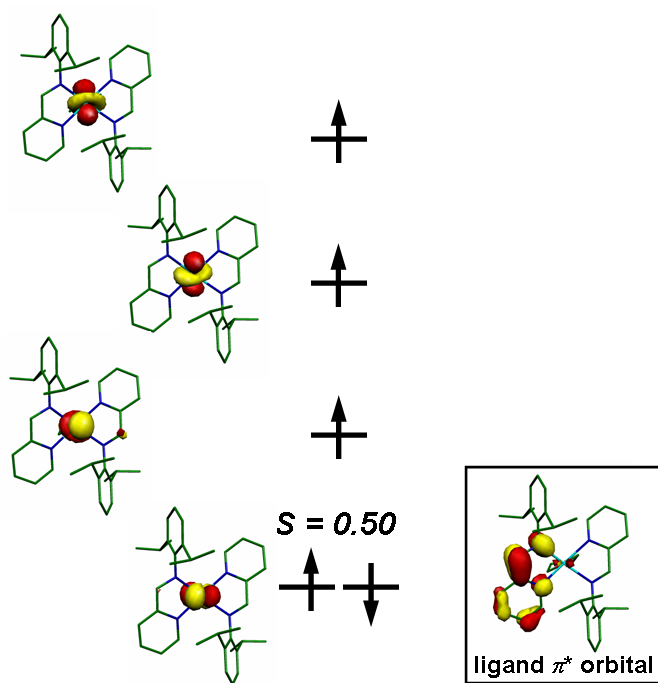
SI Figure 14. X-band EPR spectrum (dX''/dB) of $\text{Zn } 6^{\text{ox}}\cdot\text{THF}$ in frozen THF (0.5 mM, 20.0 K, frequency = 9.45 GHz, modulation = 6.0 G, power = 200 μW).



SI Figure 15. Qualitative MO diagram of the magnetic orbitals derived from the BS(4,2) calculation of the Cr complex **1**. The spatial overlaps (S) of the corresponding alpha and beta orbitals are given. The last unoccupied d-orbital was not located.

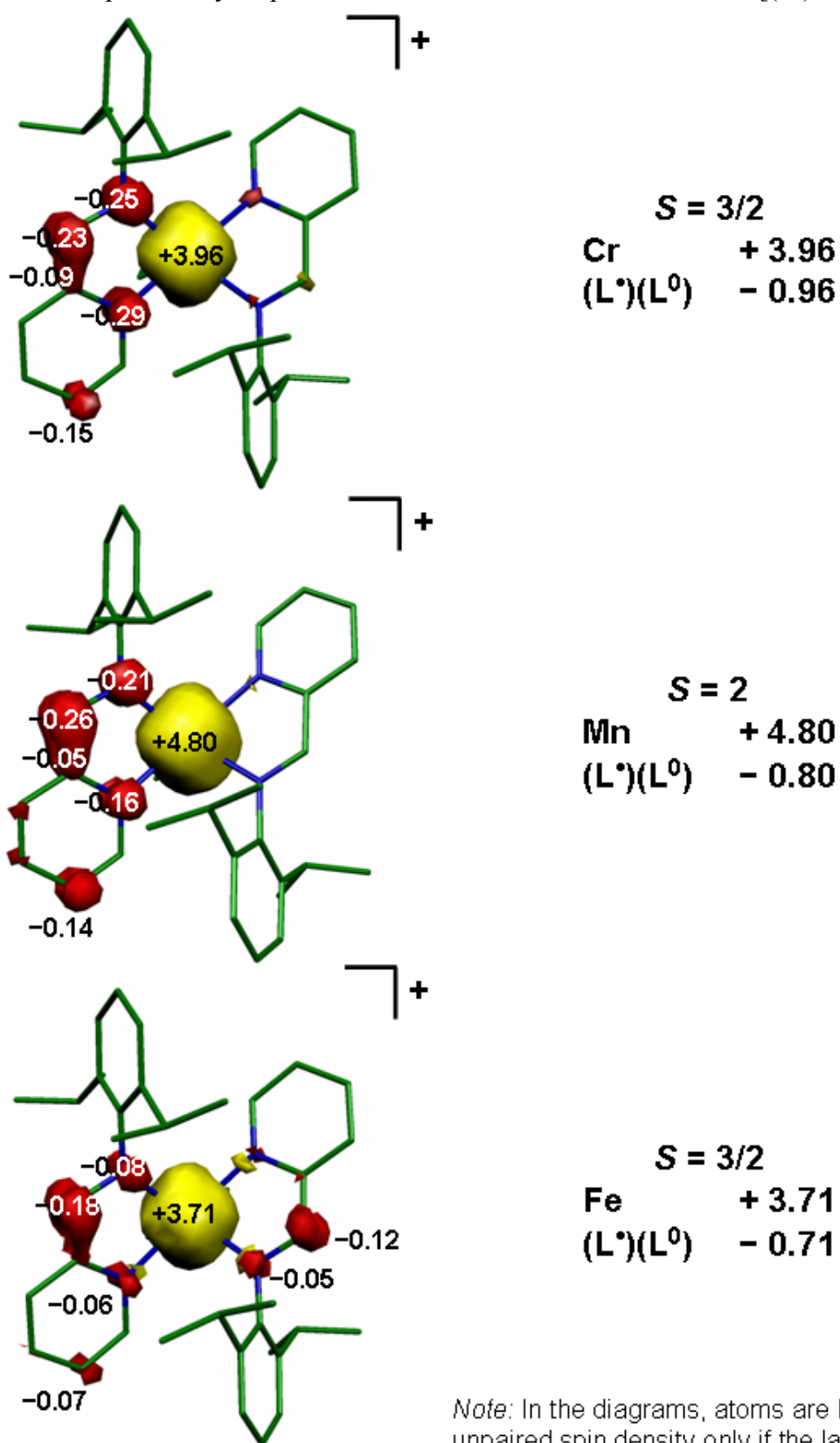
SI Figure 16. Spin density distribution for DFT models of Zn 6^{0x} ·THF that consider solvation effects using COSMO. ϵ is the dielectric constant of the solvent. Only atoms with spin densities ≥ 0.05 are labeled.



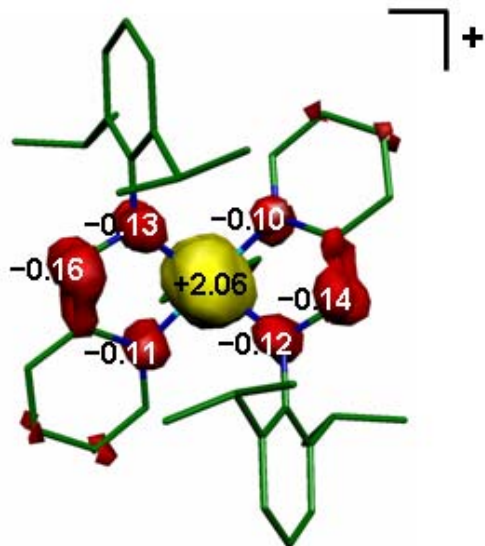


SI Figure 17. Qualitative MO diagram of the magnetic orbitals derived from BS(4,1) calculation of $[(L^*)(L)_2Cr(THF)]^+ \mathbf{1}^{ox} \cdot THF$. The spatial overlap (S) of the corresponding alpha and beta orbitals is given. The last unoccupied d-orbital was not located.

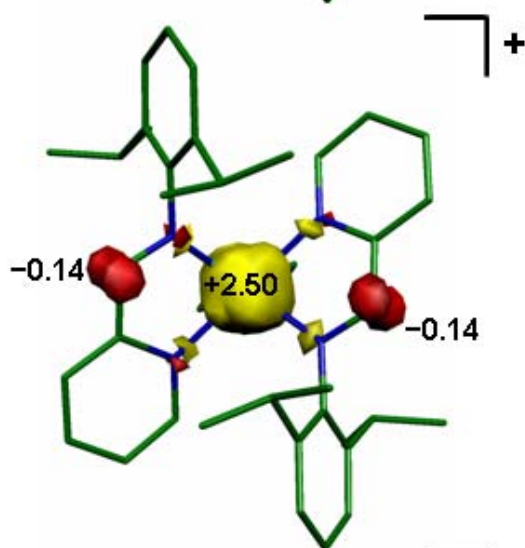
SI Figure 18. Spin density maps of the DFT models of the cationic series $[(L^*)_2M(THF)]^+$.



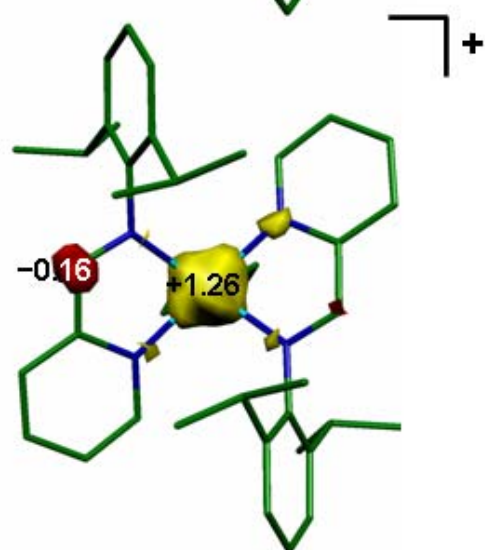
Note: In the diagrams, atoms are labeled with their unpaired spin density only if the latter is ≥ 0.05 .



$S = \frac{1}{2}$
Fe + 2.06
(L*)(L⁰) - 1.06



$S = 1$
Co + 2.50
(L*)(L⁰) - 0.50



$S = \frac{1}{2}$
Ni + 1.26
(L⁰)₂ - 0.26

Note: In the diagrams, atoms are labeled with their unpaired spin density only if the latter is ≥ 0.10 .